UC Davis

UC Davis Previously Published Works

Title

Characterization, analysis, and implementation of integrated bandstop structures on ultra-wideband archimedean spiral antenna

Permalink

https://escholarship.org/uc/item/98733110

Journal

IEEE Transactions on Antennas and Propagation, 64(5)

ISSN

0018-926X

Authors

Jeon, JH
Chang, JT
Pham, AV

Publication Date

2016-05-01

DOI

10.1109/TAP.2016.2539368

Peer reviewed

eScholarship.org Powered by the California Digital Library
University of California

Characterization, Analysis, and Implementation of Integrated Bandstop Structures on Ultra-wide Band Archimedean Spiral Antenna

Jae H. Jeon, John T. Chang, and Anh-Vu Pham

***Abstract*—A subsection of the radiating spiral arm, placed in parallel, induces a bandstop response at a notch frequency proportional to the resonant length of the strip. Detailed parametric study on the effect of variation of design parameters for an Archimedean spiral antenna and the resonant parallel strip (RPS) is presented. Empirical analysis on phase velocity on the radiating spiral arms allows characterization of RPS in terms of its resonant length. Identified systematic relation between design parameters and filter response is applied to design an antenna for the 3.1 – 10.5 GHz operating band with the notch response over the IEEE 802.11a band, 5.15 to 5.95 GHz. Successful implementation is demonstrated through performance comparison between simulated and experimental results.**

***Index Terms*—Bandstop filters, notch filters, spiral antennas, ultra wideband**

I. Introduction

Federal communication committee (FCC) designated ultra-wideband (UWB) spectrum with a strict spectral mask requirement on the transmitter output to ensure proper interoperability with other narrowband wireless standards occupying the spectrum [1]. The wideband attribute of receivers on UWB systems lead to potential susceptibility to interference from RF sources in proximity that share the portion of the UWB spectrum. Component filters can be integrated into the front-end circuit to mitigate the interference at the expense of added cost and increased size. However, the availability of component filters in the commercial market has selective limitation in its frequency range. Microstrip filters can be designed but its size becomes unwieldy for the frequencies in the UWB spectrum. Another method of mitigation is to integrate a desired filter response in the antenna performance. Planar microstrip monopole is a widely used type of UWB antenna [2]. Secondary resonant structures (SRS) can be designed in into planar monopoles such that the current path around SRS corresponds to quarter wavelength of the notch frequency, inducing a stopband response [3]. Literature is replete with examples of successful implementation of such technique [4].

Theoretically frequency independent nature allows practical implementation of spiral antennas for wideband applications in a compact size [5]. Slits in the spiral arms have been observed to induce a stopband response [6]. Another method to induce spectrally localized impedance mismatch over the 802.11a band, and simultaneously in the 3.4 GHz band, has been successfully demonstrated for spiral antennas designed to operate in the UWB spectrum [7], [8]. A parallel spiral strip, placed on the opposite side of the substrate as the radiating spiral arms, couples energy at a certain frequency band, allowing it to be characterized by its resonant length. Similar structure is known to increase the operating bandwidth of the antenna [9]. The advantages of using RPS over slits are that it can be easily tuned in post fabrication and that the RPS layer can be printed separately and be conjoined impermanently. In this paper, a detailed parametric study is conducted on RPS and its effect on antenna performance. Empirical analysis, and design method are developed and presented in this paper along with a successful demonstration through experimental results.

Manuscript accepted on January 31, 2016. This work performed under the auspices of the U.S. Department of Energy by Lawrence Livermore National Laboratory under Contract DE-AC52-07NA27344.

John T. Chang is with the Lawrence Livermore National Laboratory, Livermore, CA 94550 USA (chang16@llnl.gov).

Anh-Vu Pham is with the Department of Electrical and Computer Engineering, University of California, Davis, Davis, CA 95616 USA (pham@ece.ucdavis.edu).

Jae H. Jeon is with both of the aforementioned organizations (jeon2@llnl.gov).

II. Antenna Design Parameter Description

A. Two-Arm Archimedean Spiral

Archimedean spiral can be interpreted as an object moving in time in a polar coordinate where the angular velocity is constant over time. This translates to the radius and the angle having a linear relationship unlike the equiangular spirals. Consequently, the radius and the angle maintain a constant spacing as well as a constant arm width as the number of turns grows. The following set of mathematical equations embodies the geometrical description:

$$\begin{aligned} \rho_1 &= \alpha\theta + \rho_0 & \rho_3 &= \alpha(\theta - \pi) + \rho_0 \\ \rho_2 &= \alpha(\theta + \delta) + \rho_0 & \rho_4 &= \alpha(\theta - \pi + \delta) + \rho_0 \end{aligned} \tag{1}$$

The constant, ρ_0, is the inner radius of the spiral antenna. This parameter controls the separation between the two opposing spiral arms at the center. The physical width of each spiral arm is controlled by the constant, δ, which is the initial angular shift. Constant impedance over frequency comes from the self-complementary nature of the antenna [10]. For spirals, the width and the spacing must be equal to be identified as a self-complementary structure [11]. α is the expansion rate of the spiral. The independent variable of the equation is the angle, θ. The range of this parameter controls the number of turns of the spiral. Typically, initial design requirements dictate how these parameters are set. Number of turns with the overall dimension of the antenna can be controlled to meet the frequency range requirement. Therefore, rather than treating the expansion rate as a separate variable, it is advantageous to describe it in terms of the other variables, as shown below:

$$\alpha = \frac{\rho_f - \rho_0}{2\pi n} \tag{2}$$

where, ρ_f designates outer radius of the spiral antenna. The total number of turns is given by, n. The first arm is modeled by using ρ_1 and ρ_2. And the second arm is given by ρ_3 and ρ_4 as

specified in (1).

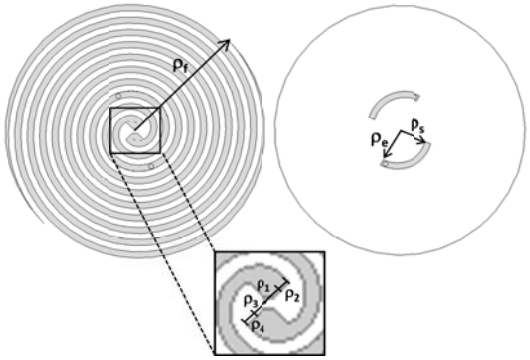

Fig 1. Dimensional drawing of an Archimedean spiral antenna with integrated bandstop structure. Main radiating arms are placed on one side of the substrate (left) and the bandstop structure is placed on the opposite side of the substrate (right).

B. Integrated Bandstop Filter Structure

Duplicate of a subsection of the main spiral is placed in parallel on the opposite side of the substrate. Dimensional depiction of the geometry is shown Fig 1. The width of RPS is the same as the main spiral width. The location and the length of RPS is described in terms of turns it takes to reach the starting and ending lateral edges of RPS:

$$\begin{aligned} \rho_s &= \alpha 2\pi n_s + \rho_0 \\ \rho_e &= \alpha 2\pi n_e + \rho_0 \end{aligned} \tag{3}$$

Parameters, n_s and n_e, designate the amount of turns to reach the starting and ending edges of RPS. Same offset and a second set shifted by 180 degrees as described in (1) can be applied to (3) to give RPS a finite width along with a symmetrical copy for the opposing arm. A via is placed at n_e on each RPS.

Two design parameters can be identified with the resonant structure: length and location. For this study, the variable n_s, corresponding to the edge closer to the center, will be referred to as the location of RPS. The length of RPS can be implicitly defined as the difference between n_s and n_e for relative comparison in the parametric study. But to gain a direct understanding of the effect of the physical length of RPS, n_e can be redefined in terms of the arc length leading up to n_s, and the arc length of RPS, l_{RPS}. Equation (1) dictates the geometry of the Archimedean spirals in terms of turns. Arc length for an Archimedean spiral is given by the following equation:

$$l_{arc} = \int_{\theta_1}^{\theta_2} \sqrt{\rho^2 + \left(\frac{d\rho}{d\theta}\right)^2}\, d\theta \tag{4}$$

Solving the integral for the arc length leading up to n_s leads to the following expression:

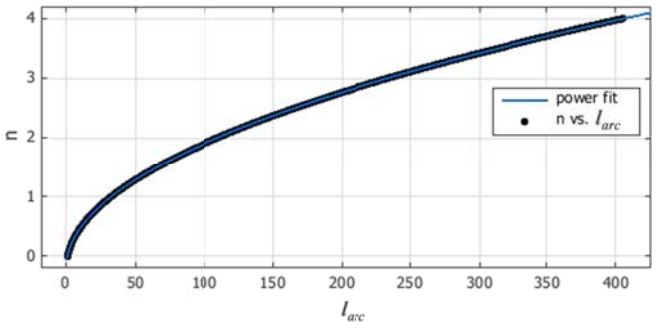

Fig 2. Plot of number of turns as a function of arc length, l_{arc}, for the following design parameters: ρ_0 = 1mm, ρ_f = 31mm = 31 mm, and n = 4.

$$l_s = \left| \frac{\frac{1}{2}\left(\alpha \log\left(\rho_0 + \alpha\theta + \sqrt{(\rho_0+\alpha\theta)^2 + \alpha^2}\right)\right) + \left((\rho_0+\alpha\theta)\sqrt{(\rho_0+\alpha\theta)^2+\alpha^2}\right)}{2\alpha} \right|_0^{\theta_s} \tag{5}$$

Once l_s is known, the combined value with l_{RPS}, can be used to define n_e. It is difficult to symbolically reverse (4) and form it in terms of arc length as the independent variable and the number of turns as the dependent variable. Numeric operation can be performed in Matlab to estimate this relationship. First, number of turns can be swept from 0 to n, and the corresponding arc lengths, l_{arc}, can be found using (4). Then, the independent variable, n, and the dependent variable, l_{arc}, are switched and plotted. Then, a curve fit operation is applied to estimate the mathematical relationship. Following second order power function with three coefficients sufficiently describes the relationship:

$$n = c_2 l_{arc}^{\ c_1} + c_0 \tag{6}$$

Fig 2 illustrates a resulting plot of this procedure for a particular set of design parameters as an example. Finally, (3) can be modified to model RPS directly in terms of desired location and characteristic length:

$$\begin{aligned} \rho_s &= \alpha 2\pi n_s + \rho_0 \\ \rho_e &= \alpha 2\pi \left[c_2 \left(l_s + l_{RPS}\right)^{c_1} + c_0\right] + \rho_0 \end{aligned} \tag{7}$$

III. Parametric Study Results

To conduct a parametric study, CST Microwave studio electromagnetic simulation software is used. Its finite integration technique (FIT) based solver is efficient for this type of broadband antenna problem [12]. There are multiple performance metrics that can be used to characterize the notch response such as S11, S21, current density on RPS, etc. Although quantitative measure differs across these metrics, presence of notch characteristics will be clearly evident in all. Therefore, only S11 is observed in this section and consideration for other metrics are deferred to the experimental section where a specific case is presented.

A. RPS Design Parameter Variation

The purpose of this section is to see the effect on the notch frequency, peak impedance mismatch at f_{n0}, and stop band bandwidth when varying the length and location of RPS. The source impedance is fixed at 140 Ohms, the total number of turns is fixed at 5, and the outer radius is set at 25 mm. RPS starting edge location is fixed at 0 turns, corresponding to the beginning of the main spiral arms. It is expected that the length of RPS inversely relates to the notch frequency. Fig 3 plots three representative cases from the result of sweeping l_{RPS}. When l_{RPS} is set at 8 mm, f_{n0} is located at 5.5 GHz. The center notch frequency shifts to 10.4 GHz as the characteristic length is reduced to 4 mm. When l_{RPS} is increased to 12 mm, f_{n0} is shifted to 3.7 GHz. Also, the secondary notch is visible at approximately 11.3 GHz, corresponding to its third harmonic. Noting f_{n0} for each case considered, the corresponding RPS length is close to one quarter of the guided wavelength:

$$l_{RPS} \approx \frac{1}{4}\frac{v_p}{f_{n0}} \tag{8}$$

The direct correlation between RPS length and guided wavelength is determined by the relative location of the via which determines the distance current travels on RPS.

With the characteristic length fixed, the result of varying the location of RPS, in terms of n_s, is shown in Fig 4. The total number of turns is 5 and the location of RPS is ranged from zero to 1.8 turns. At zero, a strong rejection at 5.5 GHz is observed. As the location is moved down the spiral, a shift in f_{n0} is evident. By 0.6 turns, it has moved up to 6.2 GHz, a difference of 700 MHz. And impedance mismatch has been decreased by about 0.4 dB in terms of S11. What is interesting is that a further movement down the spiral reverses the trend. By 1.2 turns, the center notch frequency shifts down to 6 GHz. Moving RPS further down the spiral results in an indistinguishable stop band. The rejection level becomes negligible that it is obscured by the overall quality of impedance matching. The reason for the reduction in peak rejection level is radiation. With a given characteristic length for RPS, from the zero turn location case, we know that the resonant frequency is 5.5 GHz. Band theory states that radiation happens when the circumference of the antenna reaches one wavelength of the frequency [13], [14]. Beyond the active region, most of the energy at that corresponding frequency is expected to be radiated. Therefore when RPS moves beyond the active region, it is expected that only negligible amount of energy is left on the main spiral arms to be rejected. This is what is observed in Fig 4. At some point down the spiral, the notch band characteristic starts to disappear, eventually making the profile of return loss curve very much resembling the case of the generic Archimedean spiral without the RPS.

First order analysis indicates that the arc length of RPS dictates the center notch frequency and the location of RPS dictates the peak rejection level and the associated notch bandwidth. However, as it was observed, the location of RPS also has effect on spectral placement of the induced bandstop

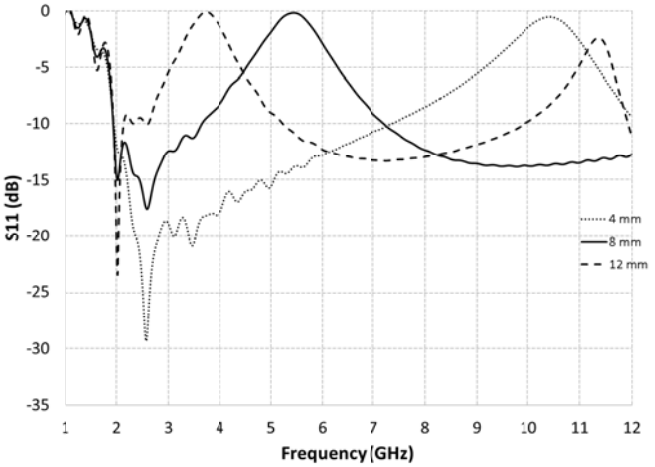

Fig 3. S11 plot of the antenna with varying characteristic length of RPS: 4 mm (dotted), 8 mm (solid), and 12 mm (dashed).

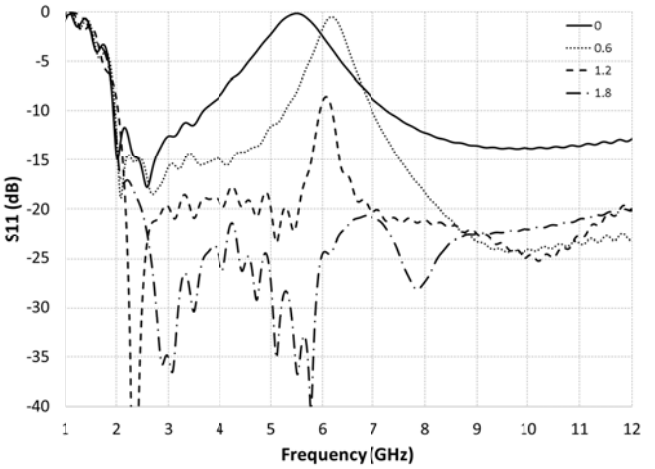

Fig 4. S11 plot of the antenna with varying location of RPS in terms of starting edge location in turns: 0 (solid), 0.6 (dotted), 1.2 (dashed), 1.8 (dash-dotted).

response. This implies that the length must vary depending on the location along the spiral, in order to keep the center notch frequency consistent. To identify how much RPS length difference there is at different locations along the spiral, RPS is moved along the spiral once again while tuning the length to maintain f_{n0} at ±20 MHz from 5.5 GHz. The resulting characteristic length at each location in terms of n_s is shown in Fig 5. Three regions can be clearly identified for all three different cases of total number of turns. In the first region, corresponding from the feed point to the location where RPS length becomes nearly constant, phase velocity ramps up which results in an increase of characteristic length for the same f_{n0}. Second region is where the phase velocity steadies resulting in a near constant l_{RPS}, considering that the standard PCB fabrication limit is about 0.2 mm. The last region begins from where the phase velocity starts to dip. In this region, the stopband response quickly diminishes, eventually becoming insignificant.

B. Main Spiral Arm Design Parameter Variation

The set of design parameters for the geometry of the main spiral arms is also expected to be a measure of influence on the

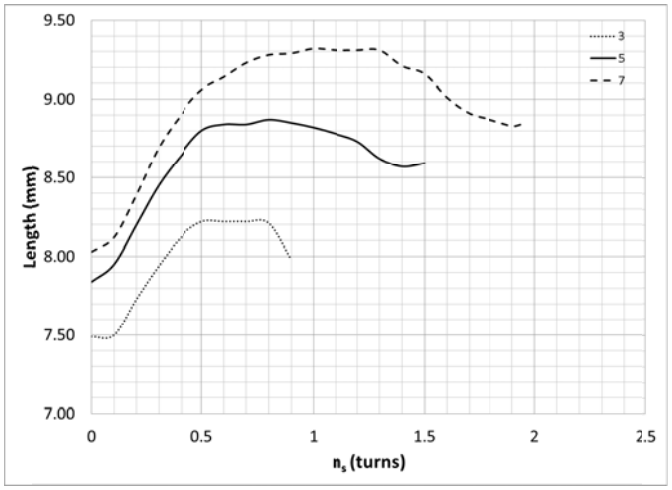

Fig 5. Characteristic length of RPS that corresponds to f_{n0} = 5.5 GHz at varying location of RPS in terms of number of turns to the starting edge for three different total number of turns: 3 (dotted), 5 (solid), 7 (dashed).

characteristic length of RPS. Spiral antenna is a slow-wave antenna [15], [16]. Individually, inner radius, outer radius, and the total number of turns all impact the phase velocity of the signal traveling down the antenna. The expansion rate, as described in (2), collectively captures the changes in these design parameters. In this section we explore a range of expansion rates and the corresponding resonant length of RPS to keep f_{n0} at 4, 5.5 and 7.5 GHz. Table 1 summarizes the values of design parameters considered and their resulting minimum feature size.

As it was noted from Fig 5, the characteristic length of RPS varies as its location is varied until it reaches a region where it becomes nearly constant. For each α, the average length in this region was noted to be the representative characteristic length. Aggregate of the resultant data points forms the plot shown in Fig 6. Also, a trend line is drawn across the data points for each series with a corresponding equation. As expected, the characteristic length varies as overall antenna design parameters are varied. Increase in α results in decrease in phase velocity, which in turn lowers the wavelength for a given frequency. Second order polynomial equations, shown in Fig 6, provide an accurate relationship between the RPS length and the expansion rate with the R^2 value greater than 0.98 in all three cases, ensuring that the error margin is less than the standard PCB fabrication limit of 0.2 mm. Comparing the 5.5 GHz and the 7.5 GHz case in Fig 6, the amount of change between the data point at α = 0.3 and α = 1.4 is 2.9 mm and 2.5 mm, respectively. This nonlinearity is attributed to the fact that the phase velocity is affected by the presence of RPS, which in turn affects the resonant length of RPS along with the changes in spiral arm width. As notch frequency shifts upwards, RPS length becomes shorter, approaching the phase velocity of the spiral antenna without the RPS.

Along with the center notch frequency, rejection level and bandwidth are also of interest when characterizing a stop band response. Location of RPS, relative to the main spirals, can be used as a design parameter that controls the level of mismatch and bandwidth of the stop band. As signal flows down the spiral from the feed point, the current density drops linearly in dB as a

TABLE I
LIST OF ANTENNA DESIGN PARAMETER VALUES

ρ_0 (mm)	ρ_f (mm)	n	α	d* (mm)
1	16	8	0.3	0.47
1	16	6	0.4	0.62
1	26	8	0.5	0.78
1	16	4	0.6	0.94
1	36	8	0.7	1.1
1	36	7	0.8	1.25
1	36	6	0.93	1.46
1	26	4	0.99	1.57
1	36	5	1.11	1.73
1	31	4	1.19	1.87
1	36	4	1.39	2.18

*d, refers to the minimum feature size of the antenna, which is equivalent to the trace width of the antenna arms: $d = \rho_1 - \rho_2 = \alpha\delta$

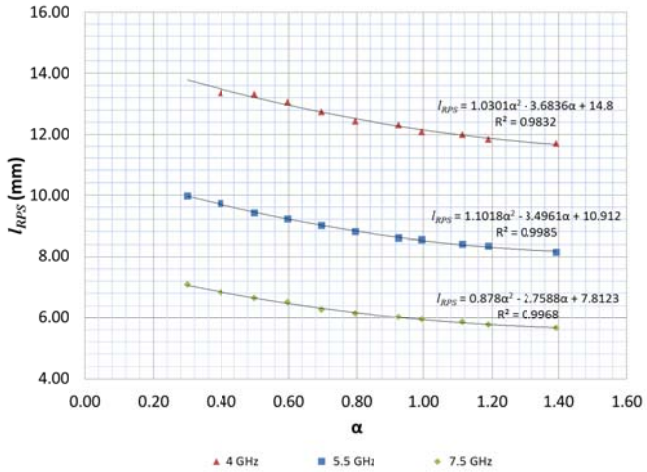

Fig 6. Characteristic length, l_{RPS}, as a function of expansion rate, α, at various notch frequencies: 4 GHz (triangle), 5.5 GHz (square), and 7.5 GHz (diamond).

function of distance [17]. Therefore it is expected that the level of rejection, in terms of impedance mismatch at the center notch frequency, will be lower as RPS is situated further away from the feed point. Three representative expansion rates are chosen for this study: 0.42, 0.55, and 0.76. For each expansion rate, the location of RPS is moved along the spiral while keeping f_{n0} tuned to 5.5 GHz, and peak VSWR and 3dB bandwidth results are determined and plotted in Fig 7. In all three cases, the impedance mismatch level falls as RPS is moved away from the center as expected since energy is being converted to radiation as the signal travels down the spiral. The associated 3 dB bandwidth narrows as RPS shifts away from center. Resultant data indicates that higher impedance mismatch and bandwidth can be achieved with lower expansion rate. While having the highest rejection level is typically desired, the relatively wide associated 3 dB bandwidth might render it less desirable. But what Fig 7 demonstrates is that a designer has the control over the antenna design parameters and the RPS location to possibly satisfy both performance requirements.

Band theory states that the active region is where the radiation happens, located at the point on the spiral where the circumference equals one wavelength. From Fig 6, it is

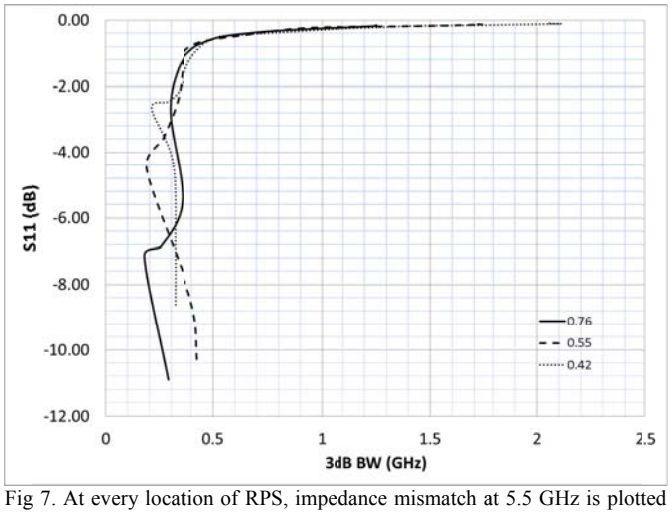

Fig 7. At every location of RPS, impedance mismatch at 5.5 GHz is plotted against associated 3dB bandwidth for various α: 0.76 (solid, n_s=0-1.5), 0.55 (dashed, n_s=0-1.94), 0.42 (dotted, n_s=0-2.45).

revealed that the phase velocity changes as antenna parameters and RPS parameters are changed. Therefore, the location of active region will depend on these design parameters. For the parameters chosen in Fig 7, the wavelength at 5.5 GHz is calculated to be 35.4 mm, 37.3 mm, 38.6 mm for α at 0.76, 0.55, and 0.42, respectively, from the equations given in Fig 6. The numbers of turns to reach the circumference equivalent to these wavelengths are 0.97, 1.44, and 1.93. And corresponding S11 levels are -0.49 dB, -0.5 dB, and -0.49 dB, which are nearly uniform. Therefore, the physical location of active region shifts as it relates to design parameters of RPS and the antenna but its electromagnetic property is maintained.

IV. Implementation of Design Method

A. Antenna Prototype Description

A five-turn Archimedean spiral with 43 mm outer diameter design was fabricated and tested in this section. The inner radius is set at 1 mm. The feed region separation is set at 0.8 mm to accommodate a balun transformer of the same material and thickness. The expansion rate is calculated to be 0.65. And the spiral width and spacing comes out to be 1.02 mm. RPS spans from 0.93 to 1.2 turns. The inner edge arc length of RPS is calculated to be approximately 9.2 mm according to the equation given in Fig 6. Vias with diameter of 0.8 mm are used. LPKF prototyping machine was used for fabrication. The final prototype of the design is shown in Fig 8.

A hole equaling the dimensions of the balun at the antenna end was drilled at the feed region of the antenna as shown in Fig 8. The hole allows the balun to be inserted into the antenna by the amount equal to the thickness of the substrate. Type of taper chosen for the balun transformer is exponential.

B. Results and Discussion

Fig 9 compares S11 simulation result between a generic and a band-notched Archimedean spiral antenna. The overall profile of impedance matching very much resembles each other in the pass band. The band-notched antenna, as designed and expected, shows a clear stop band centered around 5.5 GHz.

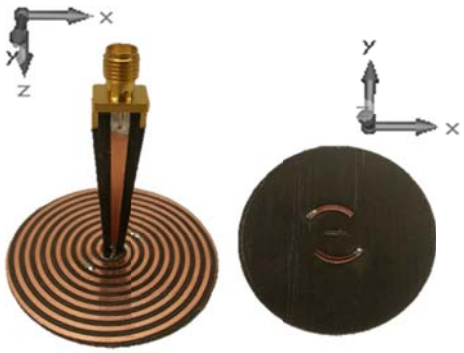

Fig 8. Picture of the fabricated prototype: Main spiral arms on top side of the substrate with the balun connection (left), and RPS on the opposite side of the substrate (right).

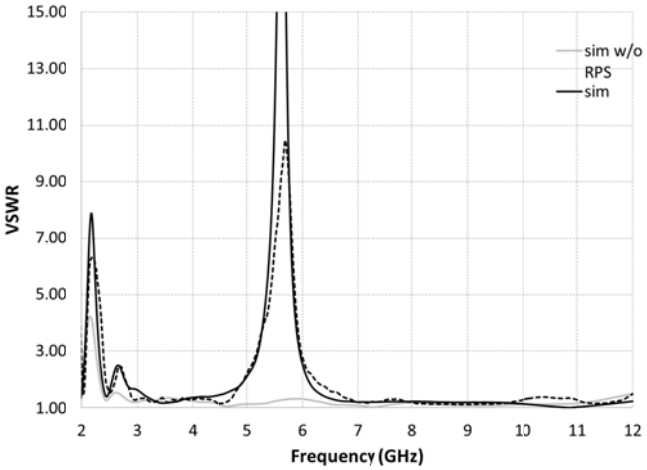

Fig 9. VSWR plot of the simulated without RPS (solid grey), simulated with RPS (solid black) and measured results (dotted).

The 10 dB crossing spans from 5 GHz to 6 GHz, covering the 802.11a band. The peak level of VSWR at 5.62 GHz is 23:1. Fig 9 also compares the simulation result and the measured result on the band notched Archimedean spiral antenna. Overall, they are in excellent agreement with each other. The center notch peak frequency for the measured result is at 5.75 GHz. The peak VSWR is 10.4:1 at f_{n0}. The 10 dB bandwidth spans from 4.95 GHz to 6.25 GHz. The lower boundary is very close with the simulation but the upper boundary is higher by about 100 MHz. The fact that a strong notch profile is seen in the S11 result leads to a conclusion that energy at the notch frequency of interest is being rejected by the antenna through the effect of RPS before it reaches the active region where radiation happens.

Fig 10 contains plots of the calculated realized gain from both simulated and the measured S21 data. As it was the case with the VSWR, the peak notch happens at 5.62 GHz in the simulation and 5.75 GHz for measured result. Simulation predicted about 10 dB drop from the passband gain. Measured result indicates stronger suppression, 18 dB drop, from the passband gain. Measured passband gain follows the simulated gain closely. Below the notchband, the gain rises from about 3 dB at 3 GHz to 4 dB at 5 GHz. Above the notchband, gain averages about 4.8 dB with the measured data, and 6 dB for the simulation data.

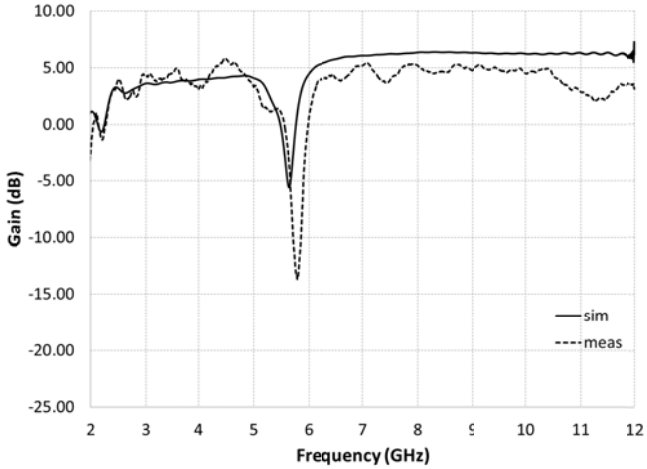

Fig 10. Boresight gain plot of the simulated (solid) and measured results (dotted).

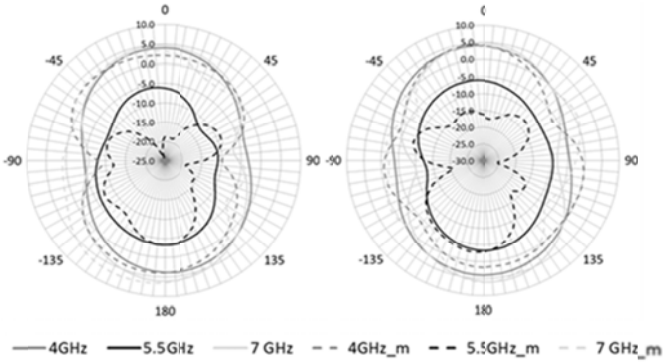

Fig 11. Simulated (solid) and measured (dotted) radiation pattern at 4 GHz, 5.5 GHz, and 7 GHz: XZ plane (left) and YZ plane (right). Antenna orientation follows the Cartesian coordinate shown in Fig 8.

To gain an understanding of the level of radiation at other angles around the antenna, a radiation pattern measurement was conducted and plotted in Fig 11. Three frequencies, 4 GHz, 5.7 GHz, 7 GHz, were selected to represent passband radiation pattern below notch frequency, notchband radiation pattern, and the passband radiation pattern above notch frequency. The general trend in the measured pattern seems to follow the simulation result. Measured radiation pattern reveals irregular levels of radiation along the 90 and -90 degree phi plane. Around zero and 180 degree theta angles, results seem much closer to the simulation result. At the notch band frequency, the radiation pattern reveals deeper nulls in non-balun side both in the XZ and the YZ plane. The difference in level of radiation is clearly visible between the tested frequencies, confirming the presence of the stop band response. Bi-directional pattern are desirable for certain wideband communication systems. Cavity, loaded with radar absorbing material (RAM), can be placed on the antenna for uni-directional beam pattern applications. In simulation, a metal cavity backing at 10 mm depth that is filled with Eccosorb FDS material with an air gap of 4 mm to the antenna was placed. Ideal balanced port was used for excitation directly to the spirals. Bandstop response, in terms of f_{n0} and 3 dB bandwidth, remained virtually the same while increasing the front-to-back ratio by 20 dB on average at the three frequencies chosen in Fig 11.

V. Conclusion

Inherently broadband nature of spiral antennas greatly appeals to UWB applications. Integrated bandstop filter response in spiral antennas provides a flexible and cost effective way of mitigating interference from in-band narrowband sources. Duplicate of a subsection of the main spiral arms, placed in parallel on the opposite side of the substrate, was shown to induce a strong spectrally localized impedance mismatch with a predictable associated bandwidth. Parametric study was conducted on the main spiral and RPS design parameters. Empirical analysis revealed its impact on phase velocity, which in turn determined the resonant length for RPS. Also, expected level of impedance mismatch at f_{n0} and 3 dB bandwidth of the notch response was analyzed. A prototype that covers the UWB spectrum while providing a notch response over the 802.11a spectrum was successfully built and demonstrated.

References

[1] Federal Communications Commission, "Revision of part 15 of the commission's rules regarding ultra-wideband transmission systems," ET Docket 98-153, FCC 02-48 pp. 1–118, Feb. 2002.

[2] Jianxin Liang; Chiau, C.C.; Xiaodong Chen; Parini, C.G., "Study of a printed circular disc monopole antenna for UWB systems," *Antennas and Propagation, IEEE Transactions on*, vol.53, no.11, pp. 3500–3504, Nov. 2005.

[3] Ki-Hak Kim; Seong-Ook Park, "Analysis of the small band-rejected antenna with the parasitic strip for UWB," *Antennas and Propagation, IEEE Transactions on*, vol.54, no.6, pp. 1688–1692, June 2006.

[4] C. Chao-Tang, L. Ting-Ju, and C. Shyh-Jong, "A Band-Notched UWB Monopole Antenna With High Notch-Band-Edge Selectivity," *Antennas and Propagation, IEEE Transactions on*, vol. 60, pp. 4492-4499, 2012.

[5] Dyson, J., "The equiangular spiral antenna," *Antennas and Propagation, IRE Transactions on*, vol.7, no.2, pp.181–187, April 1959.

[6] H. Nakano, T. Nakamura, and J. Yamauchi, "Equiangular spiral antenna with a stop band," *2nd Asia-Pacific Conference on Antennas and Propagation*, pp. 1-2, Chiang Mai, Thailand, August 2013.

[7] Jeon, J.H.; Chang, J.T.; Anh-Vu Pham, "Band-notched UWB equiangular spiral antenna," *Antennas and Propagation Society International Symposium (APSURSI), 2014 IEEE*, vol., no., pp. 1323–1324, 6-11 July 2014.

[8] Jeon, J.H.; Chang, J.T.; Anh-Vu Pham, "Archimedean spiral antenna with an integrated dual bandstop response," in *Antennas and Propagation & USNC/URSI National Radio Science Meeting, 2015 IEEE International Symposium on* , vol., no., pp.1984-1985, 19-24 July 2015.

[9] M. M. Neel, "Asymmetric antenna incorporating loads so as to extend bandwidth without increasing antenna size," U.S. Patent 6266027, July 24, 2001.

[10] Y. Mushiake, "Constant-Impedance Antennas", *J. IECE Japan*, vol. 48, no. 4, pp. 580–584 1965.

[11] V. H. Rumsey, "Frequency Independent Antennas", *1957 IRE National Convention Record*, pp. 114–118 1957.

[12] Munteanu, I; Hanninen, I, "Recent advances in CST STUDIO SUITE for antenna simulation," *Antennas and Propagation (EUCAP), 2012 6th European Conference on*, vol., no., pp.1301–1305, 26-30 March 2012.

[13] R. Bawer and J.J. Wolfe, "The spiral antenna", *IRE International Convention*, pp. 84–89, New York, March 1960.

[14] J. A. Kaiser, "The Archimedean two-wire spiral antenna," *IRE Trans. Antennas Propag.*, vol. AP-8, no. 5, pp. 312–323, May 1960.

[15] Cubley, H.; Hayre, H., "Radiation field of spiral antennas employing multimode slow wave techniques," *Antennas and Propagation, IEEE Transactions on*, vol.19, no.1, pp. 126–128, Jan 1971.

[16] Nakano, H.; Nogami, K.; Arai, S.; Mimaki, H.; Yamauchi, J., "A spiral antenna backed by a conducting plane reflector," *Antennas and Propagation, IEEE Transactions on*, vol.34, no.6, pp. 791–796, Jun 1986.

[17] Yu Yeh; Mei, K., "Theory of conical equiangular-spiral antennas: Part 2--Current distributions and input impedances," *Antennas and Propagation, IEEE Transactions on*, vol.16, no.1, pp. 14–21, Jan 1968.